

# Thermodynamic Behavior of Molecular-Scale Quantum-Dot Cellular Automata (QCA) Wires and Logic Devices

Yuliang Wang and Marya Lieberman

**Abstract**—Quantum-dot cellular automata (QCA) offers a new paradigm for molecular electronics, a paradigm in which information transmission and processing depend on electrostatic interactions between charges in arrays of cells composed of quantum dots. Fundamental questions about the operational temperature and functional gain of devices built from molecular-scale QCA cells are addressed in this paper through a statistical-mechanical model based on electrostatic interactions. The model provides exact solutions for the thermodynamic constraints on operation of small arrays of cells (up to 15). An Ising approximation dramatically reduces the computational task and allows modeling of the thermodynamic behavior of semi-infinite QCA wires. The probability of getting the correct output from a QCA device for a given input depends on temperature, cell size, cell–cell distance, effective dielectric constant of the medium, and the number of cells in the array. Using parameters derived from molecular candidates for QCA cells, the statistical–mechanical model predicts that majority gates should give correct output at temperatures of up to 450 K, while wires of thousands to millions of QCA cells are predicted to operate as functional devices at room temperature.

**Index Terms**—Ising approximation, molecular electronics, quantum-dot cellular automata (QCA), statistical mechanics, thermodynamic behavior.

## I. INTRODUCTION

THE DEMAND for denser and faster integrated circuits has inspired serious efforts to develop nanoelectronic and molecular electronic devices. With the use of molecules, nanoparticles, and nanotubes as components, the ultimate desire for molecular electronics is to achieve further miniaturization, greater functionality, and faster clock rates for advanced electronic systems, all at highly reduced cost. Recently, there have been a number of major breakthroughs in the fabrication and demonstration of nanometer-scale molecular electronic components [1], among which the quantum-dot cellular automata (QCA) proposed and demonstrated by Lent have been considered as a potential model for a future computational paradigm [2]. From the theoretical point-of-view, the idea of cellular automata (CA) was introduced in the late 1940s by von

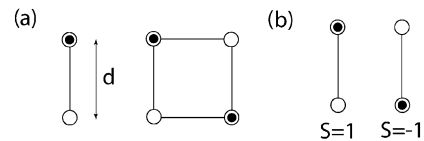


Fig. 1. (a) Schematic two- and four-dot QCA cells. The circles represent the quantum dots, the dark circles represent the location of the extra charge, and  $d$  is the separation between dots within the cell. (b) Depending on where the extra electron in a two-dot cell resides, two energetically equivalent configurations, denoted as  $S = -1$  and  $S = +1$ , can be produced. These electron configurations are used in the QCA paradigm to encode binary information.

Neumann [3] and Ulam. In the late 1960s, Conway developed the *Game of Life* [4], which simulated CA by modeling the interaction of cells following easy rules. Depending on the arrangement of cells and the rules, these arrays can perform general-purpose computation functions. The trick has been to translate arbitrary mathematical rules into a physical device that can scale to molecular sizes.

In the QCA paradigm, each cell is composed of either two or four quantum dots, as shown in Fig. 1(a), with mobile charges occupying half of the quantum dots. The four-dot cells can be regarded as paired two-dot cells. In the ground state, in the absence of external electrostatic perturbation, the two electrons in a four-dot QCA cell will adopt one of the energetically degenerate diagonal configurations shown in this figure. We use polarizations  $S = -1$  and  $S = +1$  to denote the two electron arrangements in the cell, as shown in Fig. 1(b). Binary bit values of “0” and “1” can also be assigned to these two different polarizations. When a cell is located near an unsymmetrical electric field, i.e., a driver, the two polarization states will no longer be energetically equivalent. A driver could be an input device, such as a scanning tunneling microscope (STM) tip, nanotube, or similar very sharp wire. Alternately, one cell could be driven by a neighboring QCA cell that is, in turn, interacting with an input device. Given a certain pattern of input perturbations, the whole array of QCA cells adopts its lowest energy configuration and, in the process, carries out a computation. In this manner, information can be transmitted and processed according to electrostatic interactions between the charges within the cells. A sensitive electrometer is used to read the output value from the output cell, which might be far distant from the input cells.

By using different physical arrangements of the cells, one can construct different types of QCA devices [5], as shown in Fig. 2. A QCA wire is shown in Fig. 2(a). The left-most cell is fixed with a polarization representing the input. The ground state con-

Manuscript received June 11, 2003; revised February 28, 2004. This work was supported by the Defense Advanced Research Projects Agency/Office of Naval Research under Grant 00014-99-0472.

Y. Wang was with the Department of Chemistry, University of Notre Dame, Notre Dame, IN 46556 USA. He is now with the Department of Chemistry, University of Washington, Seattle, WA 98195 USA (e-mail: yuliang@u.washington.edu).

M. Lieberman is with the Department of Chemistry, University of Notre Dame, Notre Dame, IN 46556 USA (e-mail: mlieberm@nd.edu).

Digital Object Identifier 10.1109/TNANO.2004.828576

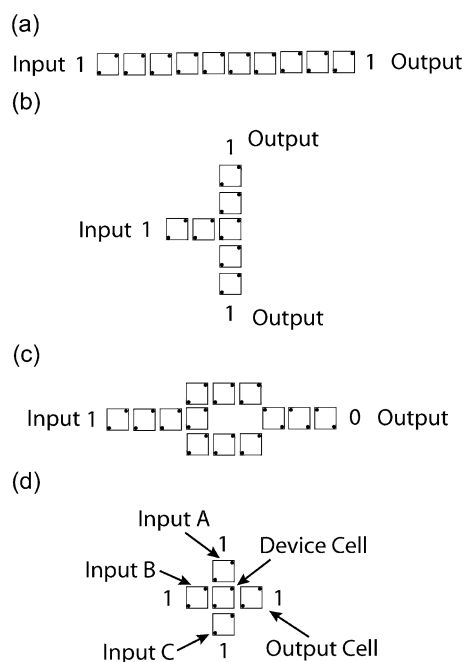


Fig. 2. QCA devices. (a) QCA wire. (b) Signal fan-out. (c) Inverter design. (d) Fundamental QCA logic device, a three-input majority gate.

figuration of the remaining free cells is then one with each cell in the line polarized in the same way as the input cell, which constitutes transmission of the input signal from one end of the wire to the other. Signal fan-out is illustrated in Fig. 2(b). Fig. 2(c) gives an inverter design. The antialignment of the input and output polarizations is a simple consequence of the mutual repulsion between electrons. The symmetric design ensures exact symmetry between the inversion of “1” and “0.” Fig. 2(d) shows the fundamental QCA logic device, a three-input majority gate, from which more complex circuits can be built. With these basic elements, logically complete computation is possible. Although the cells in these devices are all shown as the four-dot variety, all of these devices can equally well be constructed using two-dot cells.

Over the past decade, the implementation of QCA devices has been experimentally investigated. Orlov *et al.*[6], [7], Amlani *et al.* [8], and Bernstein *et al.* [9] have successfully fabricated arrays of aluminum quantum dots to demonstrate the operation of QCA wires, majority gates, clocked memory latches, and a shift register. The operating temperatures for these micrometer-scale QCA devices were approximately 80 mK. Since the electrostatic interactions between cells become stronger the smaller the cells are made, room-temperature (RT) operation of 1–10-nm scale QCA devices could be feasible.

Serious efforts now have been carried out toward the molecular implementation of QCA [10]. Instead of using traditional semiconductor material to make these very small cells, molecules have been chosen and used for investigation. The advantages of molecular QCA cells (besides the potential for RT operation) are that the cells are structurally homogeneous down to the atomic level, and that circuits can be built at an estimated density of up to  $10^{13}$  devices per  $\text{cm}^2$ .

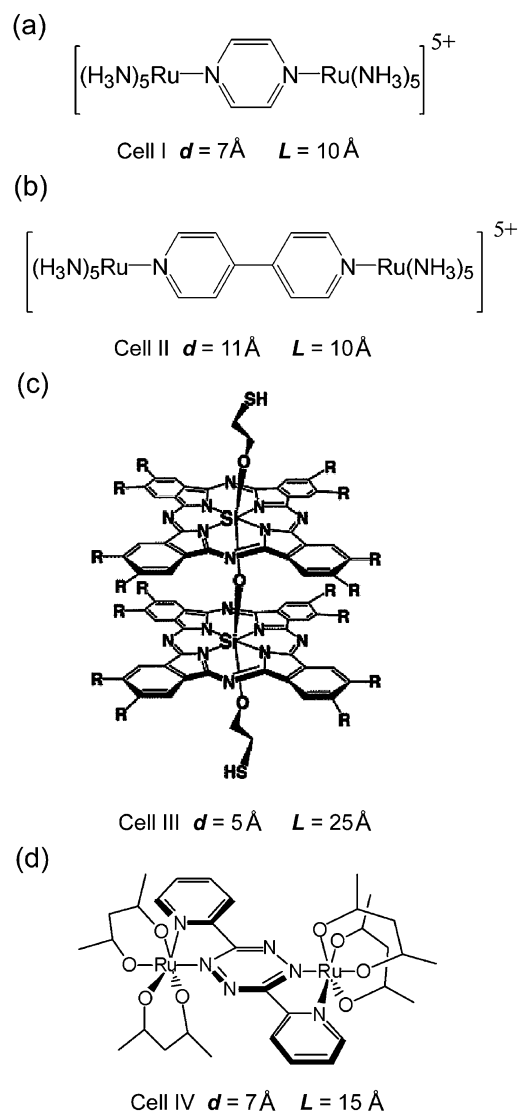


Fig. 3. Four molecular QCA candidate cells. Cell **I** and Cell **II** are the well-known Creutz–Taube ion and its 4, 4′-bipyridine analog. Both are pentacations. Cell **III** is a silicon phthalocyanine dimer. The electron can hop back and forth between the two rings. Cell **IV** is another diruthenium mixed-valence compound with an overall charge of +1. For all these four molecules, the simplified dot–dot distance  $d$  and the estimated cell-cell distance  $L$  are also shown.

The most promising molecular analogs of QCA cells consist of mixed-valence metal dimers, which are analogous to two-dot QCA cells. Two redox centers that serve as “quantum dots” are connected via a bridging ligand, which functions as a tunneling junction. Several such mixed-valence molecules are shown in Fig. 3. The distances between the two redox centers in each molecule and the estimated cell-cell spacing (based on structural modeling results using Chem 3D Ultra 8.0, CambridgeSoft, in the case of the ruthenium dimers I, II, IV, and on STM measurements in the case of the silicon phthalocyanine dimer III) are also given in this figure. Compounds I and II are the well-known Creutz–Taube ion and its 4, 4′-bipyridine analog [11], [12]. Both species are pentacations. Compounds III and IV were recently synthesized by our group [13], [14] as part of an effort to reduce the net molecular charge on the MQCA cell; they are both monocations.

Devices based upon QCA principles will only function up to a certain temperature before thermal energy causes mistakes in electron localization. The total number of cells in the devices will also affect the accuracy of the output of the devices since more mistake states are possible (entropic contribution). Intensive investigation has been carried out to model the behavior of electrons in QCA systems. Due to the operation principal of the basic device, most of these studies dealt with the ground states of the system using quantum mechanical methods [15], [16]. Tougaw and Lent recently did a dynamic behavior study for QCA wires based on traditional semiconductor-sized (20 nm) dots and molecular-sized (2 nm) dots. The results showed an improvement of the switching speed for the molecular-sized cells by a factor of 100 over the semiconductor-sized cells [17]. In addition, improvements in the possible operating temperature are predicted; the larger Columbic energies present in the molecular-sized cells make it possible for them to operate at or above RT.

In this study, we investigated the total number of QCA cells that could function together in a device before thermal fluctuations caused errors in the output. Statistical mechanics methods are used to examine the details of these thermodynamic behaviors for the many-cell molecular-sized QCA devices. By considering all the possible energy states of the devices and, thus, constructing their partition function, the expectation values for the output cells of wires and majority gates at different temperatures were obtained. The dependence of the output on the dimensions and spacing of the molecular QCA cells and the number of cells within the devices can be modeled in this way in order to probe the feasibility of molecular QCA.

## II. MODEL QCA SYSTEMS

### A. Molecular QCA Cells

Due to the equivalence of the two- and four-dot cells within the QCA paradigm, we only considered two-dot model cells. Molecular QCA cells were modeled as follows: the two redox centers in each of the candidate molecules were treated as quantum dots separated by a distance  $d$ . Every cell contains one mobile electron that is restricted to the quantum dots. The electron can hop back and forth from one site to the other, but is not allowed to leave the two-dot cell.<sup>1</sup> Polarizations  $S = -1$  and  $S = +1$  are used to denote the two electron arrangements in the cell (as shown in Fig. 1). The term polarization refers only to the arrangement of charge and does not imply a dipole moment for the cell. In our model, the driver is represented by selecting one cell as an input cell and setting its polarization to  $-1$  or  $+1$ . The driver is maintained at this polarization and

<sup>1</sup>Mixed-valence compounds can undergo a disproportionation reaction in which one dimer oxidizes another while being itself reduced; this would destroy the necessary mixed-valence charge state for QCA operation. Each of these compounds has been characterized electrochemically in order to assess the thermodynamic stability of the mixed-valence charge state to disproportionation. For compound I, the mixed-valence charge state is sufficiently stable that fewer than one molecule in 1000 will undergo disproportionation, while for compounds III and IV, fewer than one in  $10^5$  molecules will undergo disproportionation in solution. Although these estimates must be extrapolated from solution measurements to surface-bound molecules, they suggest that large ensembles of MQCA cells would be stable to disproportionation.

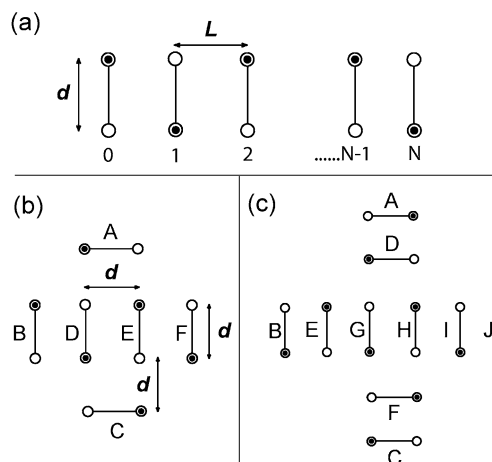


Fig. 4. Molecular QCA model. (a) MQCA wire.  $L$  is the distance between the cells and  $d$  is the distance between dots in a cell. Cell 0 is the input cell, cell  $N$  is the output cell, and there are  $(N + 1)$  cells in the line. (b) Six-cell majority gate model. Cells A–C represent the input cells, cells D and E make up the decision cell, and cell F is the output cell. The distances between dots in a cell and between cells are identical. (c) Ten-cell gate model. Cells A–C are the input cells, cells G and H make up the decision cell, and cell J is the output cell.

the other QCA cells are allowed to change their polarization in response to the fixed driver.

### B. QCA Wire

A QCA wire is represented by a line of two-dot QCA cells, as shown in Fig. 4(a). Cell  $N$  on the left-hand side is the driver cell, which is held at a fixed polarization ( $-1$  or  $+1$ ), and all the other cells in the array are free to react to this polarization. The cell on the right-hand side is the output cell. The ground state of the wire of two-dot cells has alternating cell polarizations. If there are even numbers of two-dot cells, the output cell has a polarization opposite to that of the input cell, while if there are an odd number of cells, the output polarization should be identical to the input polarization. In practice, the output value will not be exactly “ $-1$ ” or “ $1$ ,” but will lie somewhere in between, depending on the temperature and distribution of energy states within the system. An output polarization of “ $0$ ” would indicate completely random output. The important parameters in this wire model are the dot–dot distance  $d$  and the cell–cell distance  $L$ . We will consider the thermodynamic behavior of two types of model cells. One is a cell in which both  $d$  and  $L$  equal 5, 10, or 20 Å; the others match the  $d$  and  $L$  parameters measured or estimated from QCA candidate molecules shown in Fig. 3. In order to know how many cells we can put into a working wire, we determined the effect of the total number of cells on the fidelity of the output through an exhaustive statistical mechanics treatment. For some cell types, this computation became burdensome due to long coherence length of the wire, and an Ising semi-infinite wire model was used, as will be discussed later.

### C. QCA Majority Gate

Fig. 4(b) presents the most fundamental of QCA logic devices: the six-cell majority logic gate, from which more complex circuits can be built. Three inputs, here coming from the top (cell A), left (cell B), and bottom (cell C), and the output

(cell F) are positioned as neighbors of a decision gate (cells D and E). The decision cells and output cell have their lowest energy state if they assume the polarization dictated by the majority of the three input cells. As in the wire, the input cells are treated as fixed drivers, while the decision cells and outputs are free to change in response to the drivers.

Besides the cell-cell distance and cell size, the effect of the total number of cells within the logic gates was also studied. A ten-cell majority gate design shown in Fig. 3(c) was used to compare the results with the six-cell model.

### III. STATISTICAL MECHANICS METHOD

In a system that contains  $N$  two-dot QCA cells, there are a total of  $2^N$  possible states, each with its own unique distribution of the  $N$  electrons. Each state has a characteristic energy (though many states are degenerate). The ratio of the probability of populating any given excited electronic state to the probability of populating the ground state is determined by the Boltzmann distribution law

$$\frac{P_{\text{Excited}}}{P_{\text{Ground}}} = e^{-(E_{\text{Excited}} - E_{\text{Ground}})/kT}. \quad (1)$$

When thermal fluctuations exceed the energy barrier between the ground state and the manifold of excited states, one or another of the excited states will be populated and the binary output value for a QCA device will not be correctly encoded.

For a system at thermodynamic equilibrium, the expectation value of an observable  $A$  can be obtained according to the following equation:

$$\langle A \rangle = \frac{1}{F} \sum_i A_i e^{\frac{E(i)}{kT}}. \quad (2)$$

Here,  $F$  is the partition function of the system;  $E(i)$  is the system energy for the  $i$ th state. In this study, we used this equation to calculate  $\langle S_N \rangle$ , the expected polarization of the output cell  $N$ .  $\langle S_N \rangle$  has the following form:

$$\begin{aligned} \langle S_N \rangle &= \frac{1}{F} \sum_{i=1, S_N=-1, 1}^q S_N e^{\frac{-E(i) S_N}{kT}} \\ &= \frac{1}{F} \times \left( \sum_{i=1}^q 1 \times e^{\frac{-E(i) S_N=1}{kT}} \right. \\ &\quad \left. + \sum_{i=1}^q (-1) \times e^{\frac{-E(i) S_N=-1}{kT}} \right). \quad (3) \end{aligned}$$

Here,  $q$  is the number of different states in the system; each state consists of a different configuration of the  $(N-1)$  electrons in the  $2(N-1)$  ‘‘dots.’’ The electron configuration in the output cell is not included. Since the electron configuration of the input cell in a QCA wire is fixed, for an  $N$ -cell wire,  $q$  equals  $2^{N-2}$ . In the majority gate model, where there are three fixed inputs,  $q$  equals  $2^{N-4}$ . The term  $E(i)_{S_N}$  in (3) is the system energy for electron configuration  $i$  when the polarization of the output cell has the fixed value of  $S_N$ , which can be either  $-1$  or  $1$ ;

depending on the probabilities for observing these two outputs,  $\langle S_N \rangle$  can range from  $-1$  to  $+1$ .

The Coulomb interaction is considered as the only interaction between cells.  $E_{m,n}$ , which represents the Coulomb interaction between the two mobile electrons in cells  $m$  and  $n$ , has the following form:

$$E_{m,n} = \frac{e^2}{4\pi\epsilon r_{m,n}}. \quad (4)$$

Here,  $\epsilon$  is the dielectric constant of the medium and  $r_{m,n}$  is the distance between the two mobile electrons in cells  $m$  and  $n$ . The energy for each state of an  $N$ -cell QCA system is

$$E(i) = \sum_{m=1}^{N-1} \sum_{n>m}^N E_{m,n}(i). \quad (5)$$

The canonical partition function  $F$  of the  $N$ -cell system can be constructed from these energy states, as shown in (6). Thus, the expected value of the output cell  $N$  can be calculated using (3).

$$F = \sum_{i=1}^q e^{\frac{-E(i)}{kT}}. \quad (6)$$

In our calculations, the mobile charge was assigned to be positive; this treatment is just for convenience and will not affect any calculation results for molecules in which the mobile charge is negative.

In order to determine the number of cells that can be integrated in a useful QCA wire, we must consider very long wires. Since the computational task increases exponentially with the number of cells considered, it is not practical to consider all pairwise interactions between every cell. In fact, the Coulomb interaction between a pair of cells decreases with the increasing distance between the cells. The Ising nearest neighbor model has been used successfully in many similar systems that have short-range interactions [18], [19]. Such an approximation can be used to obtain an analytical expression for  $\langle S_N \rangle$  for a semi-infinite wire, as shown below.

If we use  $S_m = 1$  to represent the electron configuration of cell  $m$  when the electron is at top site and  $S_m = -1$  to describe the electron at the bottom position in the QCA wire, the pairwise Coulomb interaction between cells  $m$  and  $n$  will be given by (7)

$$\begin{aligned} E_{m,n} &= \left( \frac{1 + S_m S_n}{2} \right) \frac{e^2}{4\pi\epsilon \sqrt{(m-n)^2 L}} \\ &\quad + \left( \frac{1 - S_m S_n}{2} \right) \frac{e^2}{4\pi\epsilon \sqrt{(m-n)^2 + a^2} L} \\ &= \frac{e^2}{4\pi\epsilon \cdot 2L} \left( \frac{1}{\sqrt{(m-n)^2}} + \frac{1}{\sqrt{(m-n)^2 + a^2}} \right) \\ &\quad + \frac{S_m S_n e^2}{4\pi\epsilon \cdot 2L} \left( \frac{1}{\sqrt{(m-n)^2}} - \frac{1}{\sqrt{(m-n)^2 + a^2}} \right) \quad (7) \end{aligned}$$

where  $a = d/L$ ,  $d$  is the distance between “dots” in the cell and  $L$  is the cell–cell distance. The total energy of an  $(N + 1)$ -cell wire system, with cell 0 as the input cell, will be

$$E = \sum_{n=1}^N E_{0,n} + \sum_{m=1}^{N-1} \sum_{n>m}^N E_{m,n}. \quad (8)$$

If we assume that each cell in the wire interacts strongly only with its nearest neighbors, then the system energy only consists of terms describing the interaction of each cell with its nearest neighbors. The final simplified expression of the system energy may be represented as shown in (9) for wire with input value “1” ( $S_0 = 1$ ) and in (10) for wire with input value “-1” as follows:

$$E = C_1 N + C_2 S_1 + C_2 \sum_{m=1}^{N-1} S_m S_{m+1} \quad (9)$$

$$E = C_1 N - C_2 S_1 + C_2 \sum_{m=1}^{N-1} S_m S_{m+1} \quad (10)$$

where

$$C_1 = \frac{e^2}{8\pi\epsilon L} \left( \frac{1 + \sqrt{1 + a^2}}{\sqrt{1 + a^2}} \right) \quad (11)$$

and

$$C_2 = \frac{e^2}{8\pi\epsilon L} \left( \frac{\sqrt{1 + a^2} - 1}{\sqrt{1 + a^2}} \right). \quad (12)$$

The partition function  $F$  of such a  $(N + 1)$ -cell semi-infinite wire will be

$$\begin{aligned} F &= \sum_i^q e^{-E(i)/kT} \\ &= \sum_{S_1=\pm 1, \dots, S_N=\pm 1} e^{-C_1 N/kT} \cdot e^{-C_2 S_1/kT} \\ &\quad \cdot e^{-C_2 S_1 S_2/kT} \dots e^{-C_2 S_{N-1} S_N/kT} \\ &= e^{-C_1 N/kT} \left( e^{C_2/kT} + e^{-C_2 N/kT} \right)^N. \end{aligned} \quad (13)$$

$\langle S_N \rangle$ , the expectation value for the polarization of the output cell  $N$ , can be then calculated as follows:

$$\begin{aligned} \langle S_N \rangle &= \frac{1}{F} \left( 1 \times \sum_{S_1=\pm 1, \dots, S_{N-1}=\pm 1} e^{-E_{S_N=+1}/kT} \right. \\ &\quad \left. + (-1) \times \sum_{S_1=\pm 1, \dots, S_{N-1}=\pm 1} e^{-E_{S_N=-1}/kT} \right) \\ &= \frac{1}{F} \sum_{S_1=\pm 1, \dots, S_{N-1}=\pm 1} \\ &\quad \cdot \left( 1 \times e^{-C_1 N/kT} \cdot e^{-C_2 S_1/kT} \right. \\ &\quad \cdot e^{-C_2 S_1 S_2/kT} \dots e^{-C_2 S_{N-1} S_N/kT} - 1 \times e^{-C_1 N/kT} \\ &\quad \cdot e^{-C_2 S_1/kT} \cdot e^{-C_2 S_1 S_2/kT} \dots e^{C_2 S_{N-1} S_N/kT} \left. \right) \end{aligned}$$

and the final expressions for  $\langle S_N \rangle$  are

$$\langle S_N \rangle = (-1)^N \left( \frac{e^{C_2/kT} - e^{-C_2/kT}}{e^{C_2/kT} + e^{-C_2/kT}} \right)^N \quad (14)$$

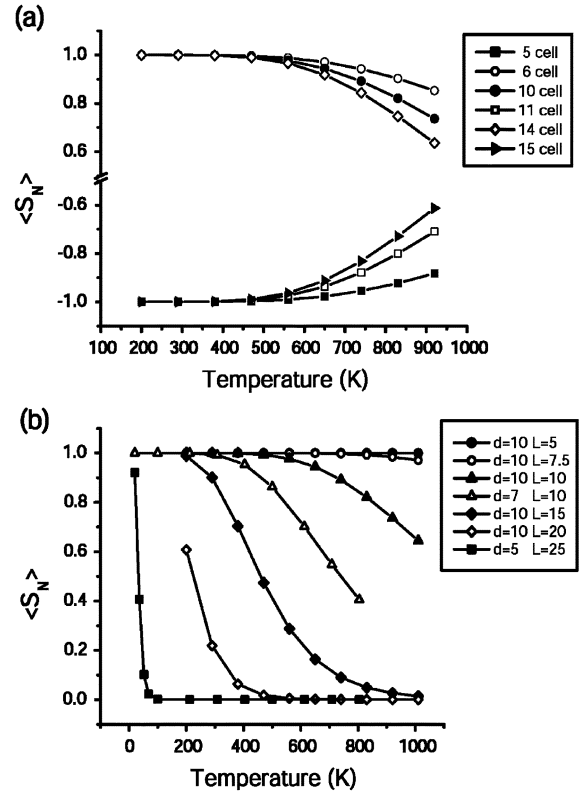


Fig. 5. Results for short MQCA wires. (a) Dependence of  $\langle S_N \rangle$  on temperature for several  $N$ -cell wires with  $d = L = 10 \text{ \AA}$ .  $N$  varies from 5 to 15. An input polarization value of  $-1$  is used so, depending on whether the total number of cells in the wire is even or odd, the sign of the expected output value will either be  $+1$  or  $-1$ . (b) The dependence of  $\langle S_N \rangle$  on temperature for ten-cell wires with different  $d$  and  $L$  values. For a given value of  $d$ , shorter cell–cell spacing  $L$  leads to more stable output. Results on wires whose cell parameters are based on current QCA molecule candidates are also shown. Molecule III with  $d = 5 \text{ \AA}$ ,  $L = 25 \text{ \AA}$  will not work when the temperature is above 30 K, but molecule I with  $d = 7 \text{ \AA}$ ,  $L = 10 \text{ \AA}$  could work up to 400 K. Generally, when  $L \geq 2d$ , the wire does not function at RT.

for an input value of “1” and

$$\langle S_N \rangle = (-1)^{N-1} \left( \frac{e^{C_2/kT} - e^{-C_2/kT}}{e^{C_2/kT} + e^{-C_2/kT}} \right)^N \quad (15)$$

for input value of “-1.”

With this analytical expression, we can examine the relationship between  $\langle S_N \rangle$  and parameters such as the number of cells in a wire, the cell dimensions, cell–cell spacing, and operating temperature.

## IV. RESULTS

### A. Complete Statistical Mechanics Treatment for Short QCA Wires

The relationship between the expectation value of the output cell  $\langle S_N \rangle$  and the temperature  $T$  for several short QCA wires with  $d = L = 10 \text{ \AA}$  are given in Fig. 5(a). The number of cells in a wire varies from 5 to 15, with shorter wires showing more robust function than long ones. The partition function and  $\langle S_N \rangle$  were obtained by the “brute-force” method where no approximation is used, rather than by the Ising method. An input value of “-1” was used for all our wire studies so the expectation value of  $\langle S_N \rangle$  switches from “-1” to “1” depending on whether

there is an odd or even number of cells in the wire. Bistable output values ( $\langle S_N \rangle \approx 1$ ) are obtained up to approximately 500 K (at which temperature real molecules would begin to thermally decompose anyway). At higher temperatures,  $\langle S_N \rangle$  approaches “0.” For longer wires,  $\langle S_N \rangle$  drops faster than for shorter wires.

Decreasing the spacing  $L$  between cells increases the bistability of the wire due to stronger Coulomb interactions between the cells. Increasing  $L$  has the opposite effect. When  $L \geq 2d$ , the ten-cell wire is predicted to fail at RT. The predicted output behaviors for two ten-cell wires with cell parameters based on current QCA molecule candidates are shown in Fig. 5(b). The results show that the molecule III with  $d = 5 \text{ \AA}$ ,  $L = 25 \text{ \AA}$  will not work when the temperature is above 30 K, but molecule I with  $d = 7 \text{ \AA}$ ,  $L = 10 \text{ \AA}$  could work up to 400 K.

### B. Statistical Mechanics Applied to Majority Gates

There are a total of eight different combinations of polarizations for the three input cells of a majority gate. Energetically, each input cell can either favor an output value of  $S = 1$  or  $S = -1$ . In order to connect the polarization input values to the majority gate decision, we introduce the concept of bit value for the inputs and outputs. The bit value assigned to each input cell and the output cell reflects which configuration of the decision cells it favors. At ground state, depending on the electron location of the two decision cells G and H, we can have two different configurations. One is that the electron in cell G is at the bottom and in cell H is at the top; the other one is the electron in cell G at the top and in cell H at the bottom. If we assign the polarization favoring the first configuration as bit value “+1,” the polarization favoring the second one will be labeled as bit value “0.” A schematic illustration of the input bit and output bit assignments for both the six- and ten-cell gate models is shown in Fig. 6(a). Here, cells A–C are the input cells for the ten-cell gate model and D–F are the input cells for the six-cell gate model. When calculating output behavior for majority gates, the electrostatic interactions between the three fixed driver cells were not included. These inputs are fixed, thus, interactions between them will not affect their polarizations. Fig. 6(b) shows the dependence of output polarization on temperature for several input combinations for each of the two majority gates. This calculation assumes QCA cells with  $d$  and  $L$  are both equal to  $10 \text{ \AA}$ . The bit values of the inputs and output are used and shown in this figure. Due to symmetry, we only show the results with the output bit value “1” here. From this figure, we can see that some input combinations are more bistable than others, for example, the input (0, 1, 1) can produce the correct output “1” at higher temperatures than the input (1, 1, 1). When the total number of cells in the majority gate changes, the bistability of the logic output also changes: for inputs (1, 1, 1) and (1, 0, 1), we see the performance of a ten-cell gate is shown to be better than a six-cell gate; however, the opposite goes for inputs (0, 1, 1) and (1, 1, 0). Smaller values of  $d$  and  $L$  yield more stable output values, as shown in Fig. 6(c), which compares expected output values for two cell sizes with  $d = L = 5 \text{ \AA}$  and  $d = L = 20 \text{ \AA}$ . This difference arises from the larger Coulomb repulsions generated between small cells.

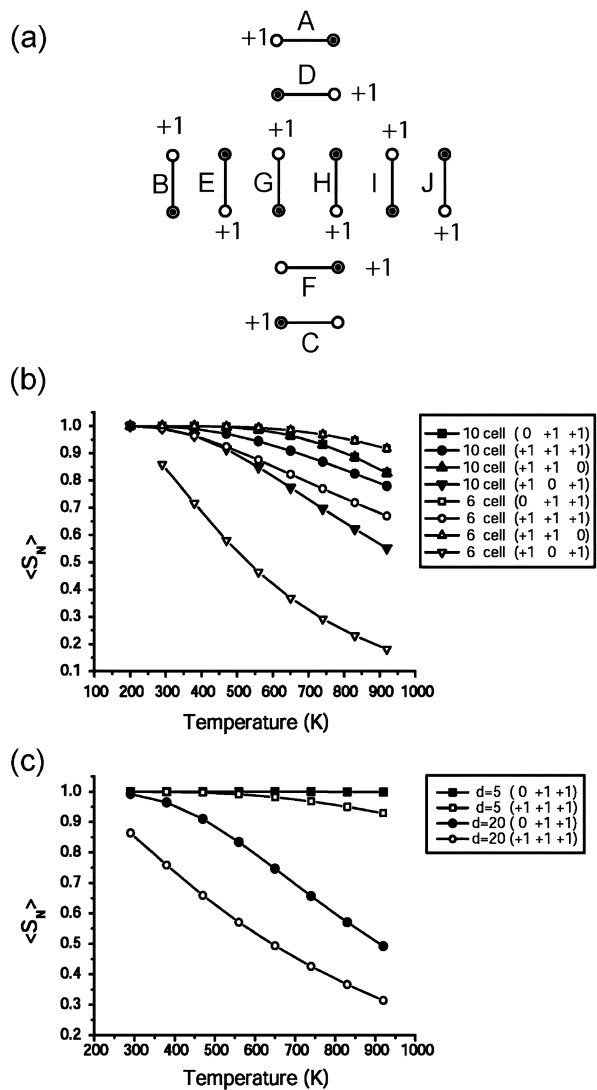


Fig. 6. Results for MQCA majority gates. (a) Input bit value assignments for the six- and ten-cell gate models. (b) Dependence of  $\langle S_N \rangle$  on temperature for the six- and ten-cell majority gate models. Since the device response is symmetric, only the four input combinations resulting in an output of “1” are shown. Identical output behaviors are obtained for inputs (011) and (110) so only one curve can be seen for these two sets of input values. (c) Dependence of  $\langle S_N \rangle$  on temperature for ten-cell majority gates with cell parameters  $d = L = 5 \text{ \AA}$  (top curves) and  $d = L = 20 \text{ \AA}$  (lower curves). The same set of inputs are used in both cases.

### C. Ising Model for Semi-Infinite Wires

We compared the value of  $\langle S_N \rangle$  for a 15-cell wire using (14) and (15) with the results obtained from (3), but with only the nearest neighbors included in the calculation; numerically, they are exactly the same. However, they are different from the results of the full calculation from (3) if all the neighbors are included because electrostatic interactions are fairly long range. The nearest neighbor approximation, which is necessary to obtain an analytical solution for the Ising model, leaves out the unfavorable interactions between the  $N$ th and  $(N + 2)$ th cells, the favorable interactions between the  $N$ th and  $(N + 3)$ rd cells, etc. The Ising results for several short QCA wires were compared with brute-force calculations that explicitly included the effects of different numbers of neighbors. Fig. 7 shows how the expectation value of  $\langle S_N \rangle$  depends on temperature for a 15-cell

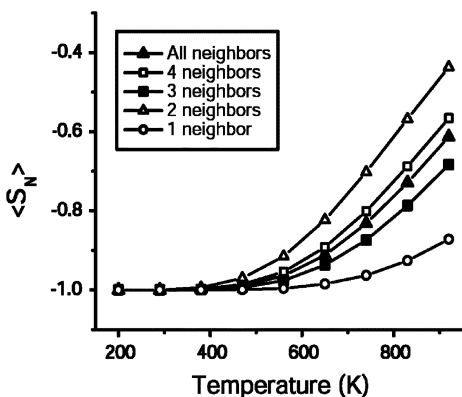


Fig. 7. Effect of nearest neighbor approximations calculated using a brute-force approach. The dependence of  $\langle S_N \rangle$  on temperature is shown for calculations in which the electrostatic effects of either 1–4 or all neighbors on each side of a cell are included.

wire when all neighbors are considered in the calculation, and when only 1–4 neighbors are considered. The nearest neighbor approximation clearly overestimates the stability of the output value. Although the deviation is small at RT for a 15-cell wire, it should be taken into consideration in interpreting our results for longer wires.

The question that we think requires the use of the Ising model despite its overoptimistic bias is: How long can a working QCA wire be at a given temperature? Here, we define a working wire as one whose output value of  $\langle S_N \rangle$  is significantly different from the “random output” value of zero. Brute-force calculations place this critical value above 15 cells for  $d$  and  $L$  values, which resemble those of molecular QCA candidates, but due to computational constraints, we could not apply brute-force methods to very long QCA wires. Fig. 8(a) gives the results [calculated from (15)] of  $\langle S_N \rangle$  dependence on the number of cells for wires with  $d = L = 10 \text{ \AA}$ . Even numbers of two-dot cells were used so when we used the fixed input “–1,” the expected output value would be “+1.” Even for a 2000-cell wire, a good output value ( $\langle S_N \rangle \sim 1$ ) is predicted for temperatures over 500 K. The inset of this figure gives another view of (15), which shows the expected output value as a function of the number of cells at a set temperature of 300 K. The solution to the Ising equation predicts that the maximum number of cells in a functional QCA wire at RT is  $\sim 1 \times 10^7$ . This represents a satisfactory level for many molecular electronics applications (e.g., a wire up to 1-cm long).

Changing the inter-dot spacing  $d$  and the cell–cell distance  $L$  in the semi-infinite wire changes its behavior greatly, as does variation of the temperature or introduction of a dielectric that can screen electrostatic interactions between the charges. In order to determine the number of cells that can function coherently in a QCA wire, we compared semi-infinite wires using a set of assumptions drawn from current molecular QCA cell candidates. The results are shown graphically in Fig. 8(b). The least stable behavior (coherence lengths  $< 100$  cells) is seen when a dielectric constant of ten was used to simulate solvent screening. This result indicates that QCA devices will need to be exposed to either air or vacuum rather than a solvent environment. Molecule I (with  $d = 7 \text{ \AA}$ ,  $L = 10 \text{ \AA}$ ) proved much

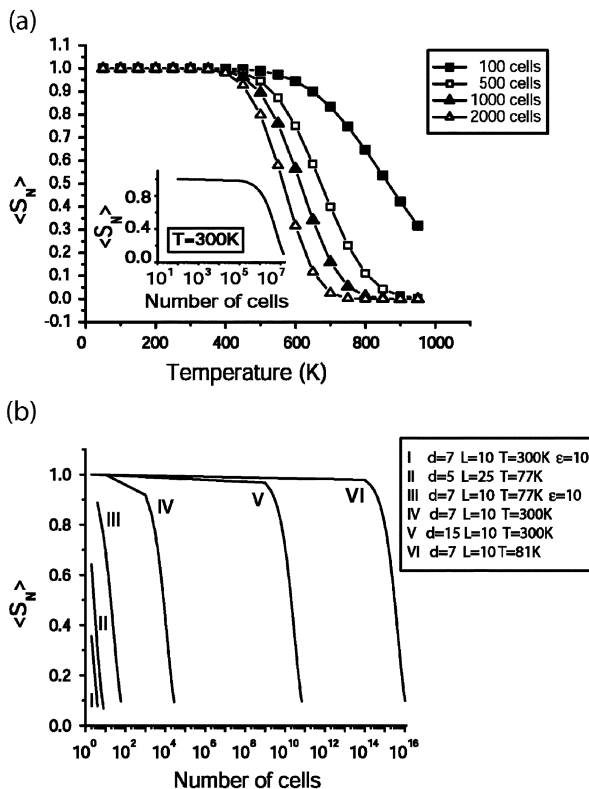


Fig. 8. Ising approximation results for semi-infinite MQCA wires. (a) Dependence of  $\langle S_N \rangle$  on temperature for several fairly long wires with cell parameters  $d = L = 10 \text{ \AA}$ . Even numbers of two-dot cells and an input polarization value of  $-1$  are used so the expected output is  $+1$ . The inset shows  $\langle S_N \rangle$  as a function of the number of cells in the QCA wire at RT. (b) Ising model results with parameters estimated from molecular systems. Dependence of  $\langle S_N \rangle$  on number of cells in a QCA wire is given for: I: Molecule I at RT in a solvent environment, II: Molecule I at liquid nitrogen temperature in a solvent environment, III: Molecule III at liquid nitrogen temperature in a solvent environment, IV: Molecule I at RT in an air or vacuum environment, V: Hypothetical molecule with long inter-dot spacing, VI: Molecule I at a liquid nitrogen temperature in an air or vacuum environment.

more promising than molecule III (with  $d = 5 \text{ \AA}$ ,  $L = 25 \text{ \AA}$ ). As expected from the results of the “brute-force” calculations in previous discussions, the long intercell distance of molecule III gave very poor output behavior and it is unsuitable for QCA wires longer than a few cells. Molecules similar to I, on the other hand, appear suitable for wires with up to 10 000 cells at RT. The number of cells that can function as a QCA wire can be greatly extended either by increasing the spacing between the dots in each cell ( $d = 15 \text{ \AA}$  rather than  $7 \text{ \AA}$  produces an estimated wire length of approximately  $10^{10}$  cells) or by lowering the temperature (liquid-nitrogen temperature rather than RT produces an estimated wire length of  $10^{14}$  cells).

## V. DISCUSSION

This paper uses basic principles of statistical mechanics to estimate functional gain for simple devices in a QCA architecture. Functional gain is defined as the number of molecular elements that can work together without necessity for amplification by the CMOS world. The amount of functional gain available for a given molecular system will be a major determinant for the ultimate device density that can be achieved—if

each molecule must be amplified by CMOS, the effective size of the molecule will be at the CMOS scale, not at the molecular scale. Molecular QCA wires and logic gates are basic devices from which more complex molecular electronic circuits would be constructed. The limitations on wires and majority gates will set fundamental constraints on more complex circuits such as adders [20] and field-programmable gate-array elements [21], which have been proposed for QCA architectures.

Clocking of QCA devices, which has been proposed by Snider *et al.* [22], [23] and demonstrated in a metal-dot system by Orlov *et al.* [24]–[26], provides power gain and pipelining to QCA circuits. In a clocked QCA architecture, the number of cells that must be “correct” would be limited to the number in each clocking region. For a QCA wire that is clocked by 20-nm CMOS wires on a 50-nm pitch, roughly 50 QCA molecules would be present in each clocking region. Our results suggest that a wire consisting of 50 QCA molecules would be workable at RT, thus, clocking of molecular QCA devices may be feasible.

The simple thermodynamic models we have developed allow variation of molecular dimensions, cell–cell spacing, and other properties that offer design guidelines for QCA molecules. Molecules with small  $L$  and larger  $d$  values are preferable for wires, while for majority gates, which basically require two wires to cross at a decision cell, it is better if  $d = L$ . Due to the difficulty of fabricating real devices from molecular components, we think it is more practical to make a single type of molecular cell (with  $d = L$ ) and use it to construct both wires and majority gates rather than to try to integrate two different cell types in different spatial positions. A newly developed technique for molecular deposition is promising for this application [27], [28].

The molecular QCA cells in this study were treated as ideal quantum dots, and we did not consider molecular properties such as thermal stability, charge delocalization onto the bridging ligand, and spin pairing of the electrons in neighboring cells. It is certain that most of the molecules we are considering would no longer be themselves at the high temperatures shown in these figures, and other factors, like surface charges or irregular spacing between cells, could reduce the performance of molecular QCA devices. Nonetheless, these simple models offer both an upper limit to the functional gain that is possible for different molecular systems, and guidance in the design of QCA molecules. Future work will be directed toward improvement of the known deficiencies of the Ising model and toward understanding the impacts of surface charge and defects in cell placement on QCA device functions.

#### ACKNOWLEDGMENT

The authors thank Prof. G. Hartland, Prof. J. Daniel Gezelter, and C. Xu, Department of Chemistry, University of Notre Dame, Notre Dame, IN, for advice and discussion on the Ising model.

#### REFERENCES

- [1] K. Kwok and J. Ellenbogen, “Moletronics: Future electronics,” *J. Mater. Today*, vol. 5, pp. 28–37, Feb. 2002.
- [2] C. Lent, “Molecular electronics: Bypassing the transistor paradigm,” *Science*, vol. 288, pp. 1597–1599, June 2000.
- [3] J. von Neumann, *Theory of Self-Reproducing Automata*, A. W. Burks, Ed. Urbana, IL: Univ. Illinois Press, 1966.
- [4] M. Gardner, “Mathematical games: The fantastic combinations of John Conway’s new solitaire game ‘life,’” *Sci. Amer.*, vol. 223, pp. 120–123, Oct. 1970.
- [5] P. Tougaw and C. Lent, “Logical devices implemented using quantum cellular automata,” *J. Appl. Phys.*, vol. 75, pp. 1818–1825, Feb. 1994.
- [6] A. Orlov, I. Amlani, G. Bernstein, C. Lent, and G. Snider, “Realization of a functional cell for quantum-dot cellular automata,” *Science*, vol. 277, pp. 928–930, Aug. 1997.
- [7] A. Orlov, I. Amlani, G. Toth, C. Lent, G. Bernstein, and G. Snider, “Experimental demonstration of a binary wire for quantum-dot cellular automata,” *Appl. Phys. Lett.*, vol. 74, pp. 2875–2877, May 1999.
- [8] I. Amlani, A. Orlov, G. Toth, G. Bernstein, C. Lent, and G. Snider, “Digital logic gate using quantum-dot cellular automata,” *Science*, vol. 284, pp. 289–291, Apr. 1999.
- [9] G. Bernstein, I. Amlani, A. Orlov, C. Lent, and G. Snider, “Observation of switching in a quantum-dot cellular automata cell,” *Nanotechnology*, vol. 10, pp. 166–173, June 1999.
- [10] M. Lieberman, S. Chellamma, B. Varughese, Y. Wang, C. Lent, G. Bernstein, G. Snider, and F. Peiris, “Quantum-dot cellular automata at a molecular scale,” in *Molecular Electronics II*. New York: New York Acad. Sci., 2002, vol. 960, pp. 225–239.
- [11] C. Creutz, “Mixed valence complexes of d5–d6 metal centers,” *Prog. Inorg. Chem.*, vol. 30, pp. 1–73, 1983.
- [12] C. Creutz and H. Taube, “A direct approach to measuring the Franck–Condon barrier to electron transfer between metal ions,” *J. Amer. Chem. Soc.*, vol. 91, pp. 3988–3989, July 1969.
- [13] S. Chellamma and M. Lieberman, “Synthesis and properties of  $[\text{Ru}_2(\text{acac})_4(\text{bptz})]^{n+}$  ( $n = 0, 1$ ) and crystal structure of  $[\text{Ru}_2(\text{acac})_4(\text{bptz})]$ ,” *Inorg. Chem.*, vol. 40, pp. 3177–3180, June 2001.
- [14] Z. Li and M. Lieberman, “Axial reactivity of soluble silicon (IV) phthalocyanines,” *Inorg. Chem.*, vol. 40, pp. 932–939, Feb. 2001.
- [15] M. Governale, M. Macucci, G. Iannaccone, C. Ungarelli, and J. Martorell, “Modeling and manufacturability assessment of bistable quantum-dot cells,” *J. Appl. Phys.*, vol. 85, pp. 2952–2971, Mar. 1999.
- [16] H. Wu and D. Sprung, “Three-dimensional simulation of quantum cellular automata and the zero-dimensional,” *J. Appl. Phys.*, vol. 84, pp. 4000–4005, Oct. 1998.
- [17] P. Tougaw and C. Lent, “Dynamic behavior of quantum cellular automata,” *J. Appl. Phys.*, vol. 80, pp. 4722–4736, Oct. 1996.
- [18] Z. Strycharski and J. Cislo, “The nonuniversal Ising model with nearest-neighbor interactions on a ferrimagnetic square lattice,” *J. Phys. C, Solid State Phys.*, vol. 21, pp. L1115–L1118, Dec. 1986.
- [19] G. Matvienko, “Critical behavior of a plane Ising antiferromagnet with two-dimensional dipole interaction,” *Theor. Math. Phys.*, vol. 69, pp. 1156–1163, Nov. 1986.
- [20] P. Tougaw and C. Lent, “Logical devices implemented using quantum cellular automata,” *J. Appl. Phys.*, vol. 75, pp. 1818–1825, Feb. 1994.
- [21] M. Niemier, A. Rodrigues, and P. Kogge, “A potentially implementable FPGA for quantum dot cellular automata,” presented at the 1st Non-Silicon Computation Workshop, Boston, MA, Feb. 3, 2002.
- [22] G. Snider, A. Orlov, I. Amlani, X. Zuo, G. Bernstein, C. Lent, J. Merz, and W. Porod, “Quantum-dot cellular automata: Review and recent experiments,” *J. Appl. Phys.*, vol. 85, pp. 4283–4285, Apr. 1999.
- [23] K. Hennessy and C. Lent, “Clocking of molecular quantum-dot cellular automata,” *J. Vac. Sci. Technol. B, Microelectron. Process. Phenom.*, vol. 19, pp. 1752–1755, Sept./Oct. 2001.
- [24] A. Orlov, R. Kumamuru, R. Ramasubramaniam, G. Toth, C. Lent, G. Bernstein, and G. Snider, “Experimental demonstration of a latch in clocked quantum-dot cellular automata,” *Appl. Phys. Lett.*, vol. 78, pp. 1625–1627, Mar. 2001.
- [25] A. Orlov, G. Toth, I. Amlani, R. Kumamuru, R. Ramasubramaniam, C. Lent, G. Bernstein, and G. Snider, “Experimental studies of clocked quantum-dot cellular automata devices,” in *58th Device Research Conf. Dig.*, 2000, pp. 157–158.
- [26] A. Orlov, I. Amlani, R. Kumamuru, R. Ramasubramaniam, G. Toth, C. Lent, G. Bernstein, and G. Snider, “Experimental demonstration of clocked single-electron switching in quantum-dot cellular automata,” *Appl. Phys. Lett.*, vol. 77, pp. 295–297, July 2000.
- [27] Q. Hang, Y. Wang, M. Lieberman, and G. Bernstein, “Molecular patterning through high-resolution polymethylmethacrylate masks,” *Appl. Phys. Lett.*, vol. 80, pp. 4220–4222, June 2002.
- [28] ———, “Selective deposition of molecules through polymethylmethacrylate patterns defined by electron beam lithography,” *J. Vac. Sci. Tech. B, Microelectron. Process. Phenom.*, vol. 21, pp. 227–232, Feb. 2003.



**Yuliang Wang** received the B.S. degree in chemical physics from the University of Science and Technology of China, Hefei, China, in 1995, and the Ph.D. Degree in physical chemistry from the University of Notre Dame, Notre Dame, IN, in 2002.

Since September 2002, he has been a Research Associate with the Department of Chemistry, University of Washington, Seattle. His research interests include molecular electronics/nanoelectronics, microelectromechanical systems (MEMS), microlithography/nanolithography, thin-film technology, surface chemistry, metallic photonic crystals, and shape-controlled synthesis of nanostructured materials.



**Marya Lieberman** received the B.S. degree in chemistry from the Massachusetts Institute of Technology (MIT), Cambridge, in 1989, and the Ph.D. degree in bioorganic chemistry from the University of Washington, Seattle, in 1994.

As a National Science Foundation (NSF) Post-Doctoral Fellow, she studied semiconductor surface derivatization and photoelectrochemistry at the California Institute of Technology. In 1996, she joined the faculty of the University of Notre Dame, Notre Dame, IN, where she is currently an Associate Professor with the Department of Chemistry and Biochemistry. She is also involved with numerous collaborations with the College of Engineering, University of Notre Dame. Her research interests are molecular-scale patterning by both top-down and bottom-up methods, molecular electronics, inorganic and organic synthesis, and electric field effects on electron transfer.